

Rotor Position-sensorless Algorithms for Direct Power Control of Rotor-tied DFIG

Rajeshkumar M. Prasad, and Mahmdasraf A. Mulla, *Senior Member, IEEE*

Abstract—In this paper, direct power control (DPC) of rotor-tied doubly fed induction generator (DFIG) is presented for the first time. First, a theoretical study is presented to acknowledge the fundamentals of DPC of rotor-tied DFIG. Thereafter, two rotor position-sensorless algorithms (RPSAs) are presented to eliminate the need of rotor position sensor. The RPSA-I is developed using the mathematical model of rotor-tied DFIG and necessitates at least four current sensors. The RPSA-II is evolved with the requirement of only two current sensors and consequently, get rid of complex computations from the algorithm. In addition to this, it is independent of all the machine parameters and stable at or near synchronous speed. Finally, the proposed scheme is tested by real-time implementation of DFIG-based wind energy conversion system (WECS) under the dynamic wind speed conditions.

Index Terms—Direct power control (DPC), rotor-tied doubly fed induction generator, sensorless control, wind energy conversion system (WECS).

I. INTRODUCTION

The doubly fed induction generator (DFIG) is widely used and covers around 50% of installed wind turbines [1]. In design process of stator-tied DFIG, first the stator is designed and accordingly the rotor outer diameter is decided. This results in lower flux density around the shaft of the rotor core compared to other parts of the core and consequently, the weight and cost of the DFIG increases [2]. A novel configuration of grid-connected to the rotor of DFIG i.e. rotor-tied is introduced in [2]. Due to effective utilization of rotor core, the rotor-tied DFIG offers reduction in size and high torque per weight ratio. There is substantial increase in efficiency of the rotor-tied DFIG because of significant reduction in the core loss of the machine [3].

The control schemes for the DFIG are classified as field-oriented control (FOC) [4], direct torque control (DTC) [5] and direct power control (DPC) [6], [7]. Fast dynamic response, reduced dependency on machine model, reduced computational complexity, and simple implementation are the advantages of DPC [8]. The FOC of rotor-tied DFIG are presented in [9]. However, the literature on DPC of rotor-tied DFIG appears to be missing although having merit over FOC and DTC. In order to fill these research gaps, DPC scheme is presented for the rotor-tied DFIG.

The DPC scheme requires the information of rotor position for the estimation of sector. The robustness of the system can be increased by position-sensorless control. In [10], rotor

The authors are with the Department of Electrical Engineering, Sardar Vallabhbhai National Institute of Technology, Surat 395007, India (e-mail: d16el001@eed.svnit.ac.in; mam@eed.svnit.ac.in).

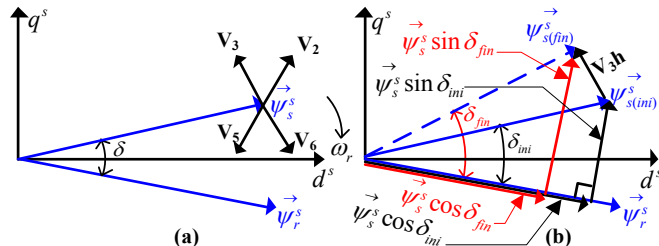


Fig. 1. Stator-flux vector variation: (a) four possible voltage vectors to modify the stator-flux location in sector 1 (b) variation in stator-flux components with V_3 injection.

position-sensorless algorithm (RPSA) is presented for the rotor-tied DFIG. This algorithm is based on complex sliding mode observer and requires PLL estimator. The design of PI controller and bandwidth of observer are the major challenges for this algorithm. Therefore, in this paper two simple RPSAs are proposed for the DPC of rotor-tied DFIG. The overall contributions of this research work for the rotor-tied DFIG are summarized as follows:

- 1) Basic control principle for the DPC of rotor-tied DFIG is presented.
- 2) The RPSA-I is formulated for the DPC of rotor-tied DFIG.
- 3) A novel sector estimation technique-based RPSA-II is presented for the DPC of rotor-tied DFIG with reduced current sensors.

II. BASIC CONTROL PRINCIPLE

In DPC scheme of rotor-tied DFIG, a two-level voltage fed inverter is used to set different voltage vectors (V_0 to V_7). These voltage vectors are applied at the stator terminal for short duration to regulate the rotor active and reactive powers. The rotor active power P_r and reactive power Q_r can be expressed by [5]

$$P_r = \frac{3}{2} \frac{L_m}{\sigma L_r L_s} \omega_e \left| \vec{\psi}_s \right| \left| \vec{\psi}_r \right| \sin \delta \quad (1)$$

$$Q_r = \frac{3}{2} \frac{\omega_e}{\sigma L_r} \left| \vec{\psi}_r \right| \left[\frac{L_m}{L_s} \left| \vec{\psi}_r \right| - \left| \vec{\psi}_s \right| \cos \delta \right]. \quad (2)$$

The desired rotor active and reactive powers can be achieved by injecting the proper stator voltage vectors and it is presented in Fig. 1. Stator-flux vector is positioned in sector 1 and moving anticlockwise as shown in Fig. 1(a). In this sector four possible vector injections are V_2 , V_3 , V_5 and V_6 . Fig. 1(b) shows the variation in stator-flux vector, after injection of V_3 .

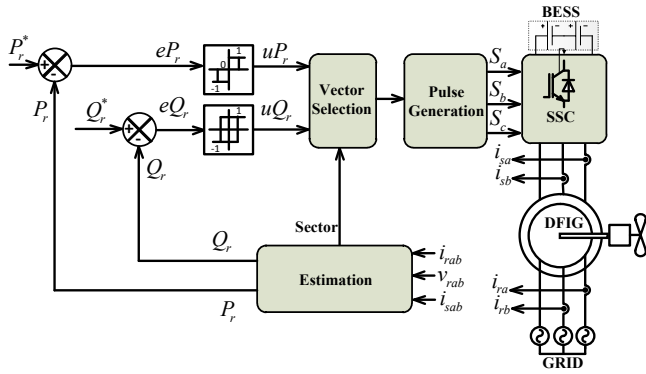


Fig. 2. Position-sensorless DPC of rotor-tied DFIG for WECS.

By assuming rotor flux rotates very slowly, during the small time interval ‘h’ rotor flux can be considered as stationary. Consequently injection of vector V_3 results to increase in magnitude of terms $|\vec{\psi}_s| \sin \delta$ and decrease in magnitude of terms $|\vec{\psi}_s| \cos \delta$ as shown in Fig. 1(b). This yields a increase in the rotor active and reactive powers, as per (1) and (2). Similarly, injections of remaining possible voltage vectors either increase or decrease the magnitude of rotor active and reactive powers. Injection of zero voltage vectors, V_0 and V_7 , results in variation of both, rotor active and reactive power.

III. CONTROL BLOCK DIAGRAM

The control block diagram of proposed DPC scheme for rotor-tied DFIG is presented in Fig. 2. The components of \vec{v}_r and \vec{i}_r in $d^r q^r$ frame can be derived as

$$\begin{bmatrix} v_{rd}^r \\ v_{rq}^r \end{bmatrix} = \begin{bmatrix} 1 & 0 \\ \frac{1}{\sqrt{3}} & \frac{2}{\sqrt{3}} \end{bmatrix} \begin{bmatrix} v_{ra} \\ v_{rb} \end{bmatrix} \quad (3)$$

$$\begin{bmatrix} i_{rd}^r \\ i_{rq}^r \end{bmatrix} = \begin{bmatrix} 1 & 0 \\ \frac{1}{\sqrt{3}} & \frac{2}{\sqrt{3}} \end{bmatrix} \begin{bmatrix} i_{ra} \\ i_{rb} \end{bmatrix}. \quad (4)$$

The rotor active and reactive power can be calculated from (3) and (4) as

$$P_r = \frac{3}{2} (v_{rd}^r i_{rd}^r + v_{rq}^r i_{rq}^r) \quad (5)$$

$$Q_r = \frac{3}{2} (v_{rq}^r i_{rd}^r - v_{rd}^r i_{rq}^r). \quad (6)$$

As shown in Fig. 2, the active power error eP_r is fed to three level hysteresis controller and reactive power error eQ_r is fed to two level hysteresis controller to get the switching states uP_r and uQ_r , respectively. The uP_r and uQ_r are defined as follows:

$$uP_r = 1, \quad \text{for } eP_r > P_{hb} \quad (7)$$

$$uP_r = -1, \quad \text{for } eP_r < -P_{hb} \quad (8)$$

$$uP_r = 0, \quad \text{for } -P_{hb} < eP_r < P_{hb} \quad (9)$$

$$uQ_r = 1, \quad \text{for } eQ_r > Q_{hb} \quad (10)$$

$$uQ_r = -1, \quad \text{for } eQ_r < -Q_{hb} \quad (11)$$

where P_{hb} and Q_{hb} are the hysteresis bands of active and reactive power, respectively.

TABLE I
SELECTION OF VOLTAGE VECTOR

$k = \text{sector}$	uP_r			
	1	0	-1	
uQ_r	1	V_{k+2}	V_0, V_7	V_{k-2}
	-1	V_{k+1}	V_0, V_7	V_{k-1}

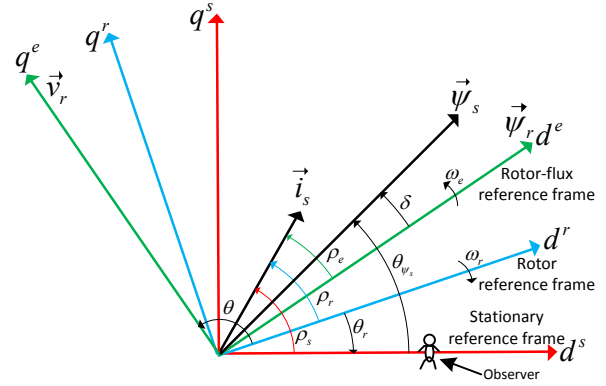


Fig. 3. Position of stator current vector with different frames.

The final voltage vectors are selected using uP_r , uQ_r and position of stator-flux vector (i.e. the sector) [5]. It is selected using look-up table of Table I. As an example, if the stator-flux vector is located in sector k , $uP_r = 1$ and $uQ_r = 1$, then the selected voltage vector is V_{k+2} . It should be noted that only four active vectors ($V_{k+2}, V_{k-2}, V_{k+1}$ and V_{k-1}) and two zero vectors (V_0 and V_7) are permitted in a particular sector.

A. Proposed RPSA-I

The phasor relation of \vec{i}_s with different frames considering the observer at stationary reference frame is presented in Fig. 3. The components of \vec{i}_s in $d^s q^s$ frame can be derived as

$$\begin{bmatrix} i_{sd}^s \\ i_{sq}^s \end{bmatrix} = \begin{bmatrix} 1 & 0 \\ \frac{1}{\sqrt{3}} & \frac{2}{\sqrt{3}} \end{bmatrix} \begin{bmatrix} i_{sa} \\ i_{sb} \end{bmatrix}. \quad (12)$$

The components of \vec{i}_r in $d^s q^s$ frame can be derived as

$$\begin{bmatrix} i_{rd}^s \\ i_{rq}^s \end{bmatrix} = \begin{bmatrix} \cos(-\theta_r) & -\sin(-\theta_r) \\ \sin(-\theta_r) & \cos(-\theta_r) \end{bmatrix} \begin{bmatrix} i_{rd}^r \\ i_{rq}^r \end{bmatrix} \quad (13)$$

$$\psi_{sd}^s = L_s i_{sd}^s + L_m i_{rd}^s \quad (14)$$

$$\psi_{sq}^s = L_s i_{sq}^s + L_m i_{rq}^s \quad (15)$$

$$|\vec{\psi}_s| = \sqrt{(\psi_{sd}^s)^2 + (\psi_{sq}^s)^2} \quad (16)$$

$$\theta_{\psi_s} = \tan^{-1} \frac{\psi_{sq}^s}{\psi_{sd}^s}. \quad (17)$$

The sector information is derived from position of stator-flux (θ_{ψ_s}). The unknown terms $\cos(-\theta_r)$ and $\sin(-\theta_r)$ used in (13) are calculated using following steps.

TABLE II
SECTOR WISE EXPECTED CHANGE IN Q_r WITH APPLICATION OF VECTORS

Sector	θ_{ψ_s}	V_0	V_1	V_2	V_3	V_4	V_5	V_6	V_7
1	$330^\circ-30^\circ$	0	-	-	+	+	+	-	0
2	$30^\circ-90^\circ$	0	-	-	-	+	+	+	0
3	$90^\circ-150^\circ$	0	+	-	-	-	+	+	0
4	$150^\circ-210^\circ$	0	+	+	-	-	-	+	0
5	$210^\circ-270^\circ$	0	+	+	+	-	-	-	0
6	$270^\circ-330^\circ$	0	-	+	+	+	-	-	0

The \vec{i}_s^r components in $d^r q^r$ frame can be computed as

$$i_{sd}^r = \frac{\psi_{rd}^r - L_r i_{rd}^r}{L_m} \quad (18)$$

$$i_{sq}^r = \frac{\psi_{rq}^r - L_r i_{rq}^r}{L_m} \quad (19)$$

The $\vec{\psi}_r$ components in the $d^r q^r$ frame are given by

$$\psi_{rd}^r = \int (v_{rd}^r - R_r i_{rd}^r) dt + \psi_{rd}^r(0) \quad (20)$$

$$\psi_{rq}^r = \int (v_{rq}^r - R_r i_{rq}^r) dt + \psi_{rq}^r(0). \quad (21)$$

Substituting the result of (20) and (21) in (18) and (19) gives

$$i_{sd}^r = \frac{\int (v_{rd}^r - R_r i_{rd}^r) dt + \psi_{rd}^r(0) - L_r i_{rd}^r}{L_m} \quad (22)$$

$$i_{sq}^r = \frac{\int (v_{rq}^r - R_r i_{rq}^r) dt + \psi_{rq}^r(0) - L_r i_{rq}^r}{L_m} \quad (23)$$

Stator current expressions in $d^r q^r$ frame as per (22) and (23) are depends on \vec{v}_r and \vec{i}_r components in $d^r q^r$ frame, which are easily calculated using sensed value of rotor voltages and currents. The unit templates of \vec{i}_s position with reference to $d^r q^r$ frame can be computed using (22) and (23) as

$$\cos \rho_r = \frac{i_{sd}^r}{\sqrt{(i_{sd}^r)^2 + (i_{sq}^r)^2}} \quad (24)$$

$$\sin \rho_r = \frac{i_{sq}^r}{\sqrt{(i_{sd}^r)^2 + (i_{sq}^r)^2}} \quad (25)$$

The unit templates of \vec{i}_s position with reference to $d^s q^s$ frame can be computed as

$$\cos \rho_s = \frac{i_{sd}^s}{\sqrt{(i_{sd}^s)^2 + (i_{sq}^s)^2}} \quad (26)$$

$$\sin \rho_s = \frac{i_{sq}^s}{\sqrt{(i_{sd}^s)^2 + (i_{sq}^s)^2}} \quad (27)$$

The unit templates of rotor position $(-\theta_r) = (\rho_s - \rho_r)$ are derived using (24) to (27) as

$$\cos(-\theta_r) = \cos \rho_s \cos \rho_r + \sin \rho_s \sin \rho_r \quad (28)$$

TABLE III
DECISION OF CHANGE IN THE SECTOR CORRESPONDING TO VARIATION IN Q_r , APPLIED VECTOR AND PRESENT SECTOR

Sector	V_0	V_1	V_2	V_3	V_4	V_5	V_6	V_7
1	0	0	-1	+1	0	-1	+1	0
2	0	+1	0	-1	+1	0	-1	0
3	0	-1	+1	0	-1	+1	0	0
4	0	0	-1	+1	0	-1	+1	0
5	0	+1	0	-1	+1	0	-1	0
6	0	-1	+1	0	-1	+1	0	0

$$\sin(-\theta_r) = \sin \rho_s \cos \rho_r - \cos \rho_s \sin \rho_r. \quad (29)$$

With the help of these unit templates, the position of stator-flux vector i.e. sector is derived using (12) to (17). The alternate and novel sector estimation scheme is presented in the next section which eliminates the need of stator currents and position sensor.

B. Proposed RPSA-II

The selection of switching vector is not depended on the exact position of stator-flux vector within the sector. Therefore, a novel sector estimation scheme is presented in RPSA-II which is based on sector wise expected change in Q_r with injection of vectors. This concept is explained with an example. Assume that stator-flux vector is moving anticlockwise for sub-synchronous operation and present sector is 1 as per the position of stator-flux vector. In this position, application of vector V_3 or V_5 and V_2 or V_6 results in increase and decrease of Q_r , respectively. If the stator-flux vector moves to sector 2, the impact of vectors V_3 and V_6 would reverse. The application of vector V_3 would now results in decrease of Q_r instead of increasing it and application of vector V_6 would now results in increase of Q_r instead of decreasing it. In both of these situations, the sector must be changed. Similarly, assume that stator-flux vector is moving clockwise for super-synchronous operation and present sector is 1 as per the position of stator-flux vector. If the stator-flux vector moves to sector 6, the impact of vectors V_2 and V_5 would reverse now. Thus for both the clockwise and anticlockwise direction of operation, at least two vectors are available which can give the information of change in sector. It is possible because the change in sector (i.e. position of stator-flux vector) will always be either +1 or -1. Table II shows the sector wise expected change in Q_r with application of vectors. If the actual change differs from expected change, then the change of sector is required. This change is either clockwise i.e. addition of -1 or anticlockwise i.e. addition of +1 and decided from Table III. The decision of change in the sector is depends on the applied vector and corresponding variation in Q_r . Therefore, it eliminates the need of stator currents and position sensor. The detail comparisons of RPSA-I and RPSA-II with existing scheme are shown in Table IV. The DPC scheme with RPSA-II requires only two current sensors for the implementation. The validation of proposed RPSAs are presented in the next section.

TABLE IV
COMPARISON OF PROPOSED RPSA-I AND RPSA-II WITH EXISTING SCHEME

Property	Existing DPC Scheme in [5], [11]	DPC Scheme with Proposed RPSA-I	DPC Scheme with Proposed RPSA-II
DFIG configuration	Stator-tied	Rotor-tied	Rotor-tied
Type of control	Rotor side control	Stator side control	Stator side control
Stator current sensors	Required	Required	Not Required
Rotor current sensors	Required	Required	Required
Flux	Rotor	Stator	Not Required
Active power	$P_s = \frac{3}{2} (v_{sd}^s i_{sd}^s + v_{sq}^s i_{sq}^s)$	$P_r = \frac{3}{2} (v_{rd}^r i_{rd}^r + v_{rq}^r i_{rq}^r)$	$P_r = \frac{3}{2} (v_{rd}^r i_{rd}^r + v_{rq}^r i_{rq}^r)$
Reactive power	$Q_s = \frac{3}{2} (v_{sq}^s i_{sd}^s - v_{sd}^s i_{sq}^s)$	$Q_r = \frac{3}{2} (v_{rq}^r i_{rd}^r - v_{rd}^r i_{rq}^r)$	$Q_r = \frac{3}{2} (v_{rq}^r i_{rd}^r - v_{rd}^r i_{rq}^r)$
d-axis Flux estimation	$\psi_{rd}^r = L_m i_{sd}^s + L_r i_{rd}^r$	$\psi_{sd}^s = L_s i_{sd}^s + L_m i_{rd}^r$	Not required
q-axis Flux estimation	$\psi_{rq}^r = L_m i_{sq}^s + L_r i_{rq}^r$	$\psi_{sq}^s = L_s i_{sq}^s + L_m i_{rq}^r$	Not required
sector estimation	$\theta_{\psi_r} = \tan^{-1} \frac{\psi_{rq}^r}{\psi_{rd}^r}$	$\theta_{\psi_s} = \tan^{-1} \frac{\psi_{sq}^s}{\psi_{sd}^s}$	From applied vector and its impact on Q_r

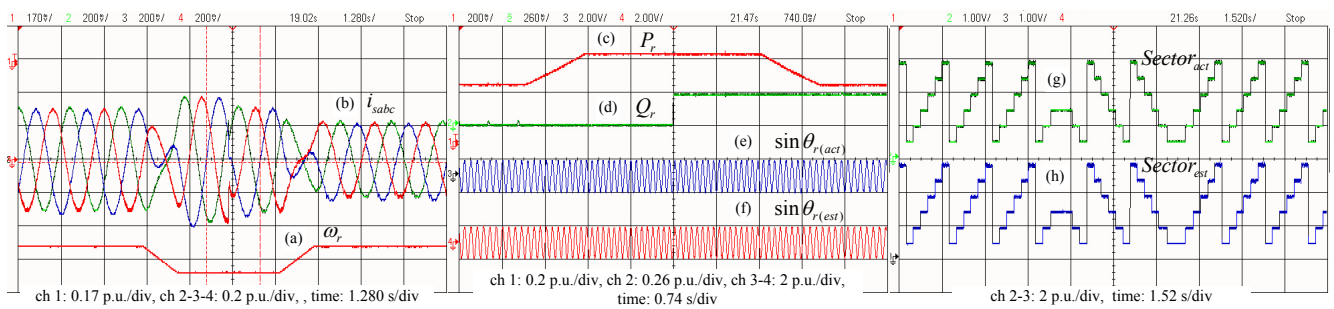


Fig. 4. Dynamic performance of rotor-tied DFIG-based WECS with RPSA-I and RPSA-II.

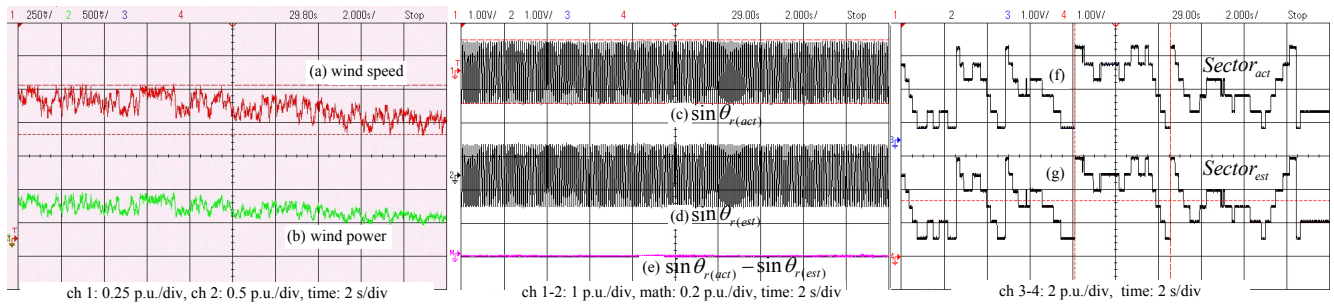


Fig. 5. Dynamic performance of RPSA-I and RPSA-II with wind speed sequence.

IV. RESULTS AND DISCUSSIONS

The proposed scheme is tested using FPGA-based XC3S5000 controller and OP-5142 real-time simulator. The controller includes 3.3-GHz processor core and working with red hat Linux platform. Total 32 channels are provided for both analog and digital input/output. The sampling frequency used for the C-code generation in FPGA is 50 kHz. Table V shows the experimental parameters of the DFIG [5]. The P_r reference is derived from wind speed. The Q_r reference is set to establish unity power factor operation at rotor side. The control parameters set in the simulation are: (a) P_r hysteresis: 2.5% of the rated power; (b) Q_r hysteresis: 2.5% of the rated power; and (c) maximum switching frequency: 5 kHz.

The variation in wind speed between 9.33 m/s and 10.66 m/s is accomplished for the validation of proposed scheme under the dynamic wind speed condition. As shown in Fig. 4(a), to extract the maximum power, the generator speed is varied between 0.933 p.u. and 1.066 p.u. The variation in stator current frequency is observed and it is shown in Fig. 4(b). The variation in phase of stator current is also observed when the generator speed changes from sub-synchronous speed to super-synchronous speed and vice-versa. The P_r reference also changes according to wind speed variation. Fig. 4(c) illustrate the P_r behaviors under this variation. A step change in Q_r reference from 0.0 p.u. to 0.24 p.u. is applied and waveform of Q_r is shown in Fig. 4(d). Due to this, the stator current

TABLE V
EXPERIMENTAL PARAMETERS OF 250 kW DFIG

Symbol	Parameters	Value
p_N	Rated power	250 kW
U_N	Stator voltage	400 V
f_N	Stator frequency	50 Hz
T_L	Rated load torque	1591 N·m
u	Stator to rotor turns ratio	1
R_s	Stator resistance	20 mΩ
R_r	Rotor resistance referred to stator	20 mΩ
L_m	Mutual inductance	4.2 mH
L_{ls}	Stator leakage inductance	0.2 mH
L_{lr}	Rotor leakage inductance referred to stator	0.2 mH
p	Number of pole pairs	2
J	Rotor Inertia	7 kg·m ²

decreases. The actual and estimated unit template of rotor position using RPSA-I are shown in Fig. 4(e) and Fig. 4(f), respectively. The estimated unit template of rotor position tracks the actual unit template of rotor position. The actual and estimated sector using RPSA-II are shown in Fig. 4(g) and Fig. 4(h), respectively. The stator-flux changes its direction with respect to $d^s q^s$ frame when generator speed alters from sub-synchronous to super-synchronous speed and vice versa, which is verified by sector numbers. The estimated sector tracks the actual sector accurately under these variation.

Fig. 5 shows the dynamic performance of RPSA-I and RPSA-II with wind speed sequence. The wind speed sequence generated from wind speed model and corresponding wind power are shown in Fig. 5(a) and Fig. 5(b), respectively. The actual and estimated unit template of rotor position using RPSA-I are shown in Fig. 5(c) and Fig. 5(d), respectively. Fig. 5(e) shows the negligible error in estimation of unit template of rotor position. The actual and estimated sector using RPSA-II are shown in Fig. 5(f) and Fig. 5(g), respectively. Overall, the experimental results endorse the proposed schemes with satisfactory performance.

V. CONCLUSIONS

The position-sensorless DPC scheme has been explored first time for the rotor-tied DFIG-based WECS. The proposed RPSA-I does not require inverse trigonometric calculations, low pass filter or proportional-integral controller to compute the rotor position, which reduces the complexity and computational time. The proposed RPSA-II requires only two rotor current sensors for the implementation. It does not require the estimations of magnitude and position of stator-flux vector. The proposed RPSA-II is independent of machine parameters and stator frequency. The performance of proposed algorithms are stable at or near synchronous speed. The presented research work have the potential to open a new direction in the field of DPC of rotor-tied DFIG.

REFERENCES

[1] R. Cardenas, R. Pena, S. Alepuz, and G. Asher, "Overview of control systems for the operation of DFIGs in wind energy applications," *IEEE Trans. Ind. Electron.*, vol. 60, no. 7, pp. 2776–2798, July 2013.
 [2] Y. You, T. A. Lipo, and B. Kwon, "Design and analysis of a novel grid-connected to rotor type doubly fed induction machine," *IEEE Trans. Magn.*, vol. 48, no. 2, pp. 919–922, Feb 2012.

[3] N. David and D. C. Aliprantis, "Improved efficiency of DFIG wind energy conversion systems by operating in the rotor-tied configuration," in *Proc. IEEE Int. Conf. ICEM*, Sept 2014, pp. 189–195.
 [4] P. Cheng, H. Nian, C. Wu, and Z. Q. Zhu, "Direct stator current vector control strategy of DFIG without phase-locked loop during network unbalance," *IEEE Trans. Power Electron.*, vol. 32, no. 1, pp. 284–297, 2017.
 [5] G. Abad, J. Lopez, M. A. Rodriguez, L. Marroyo, and G. Iwanski, *Doubly Fed Induction Machine: Modelling and Control for Wind Energy Generation*. Piscataway, NJ, USA: Wiley-IEEE Press, 2011.
 [6] H. Nian and L. Li, "Direct power control of doubly fed induction generator without phase-locked loop under harmonically distorted voltage conditions," *IEEE Trans. Power Electron.*, vol. 33, no. 7, pp. 5836–5846, 2018.
 [7] R. Datta and V. T. Ranganathan, "Direct power control of grid-connected wound rotor induction machine without rotor position sensors," *IEEE Trans. Power Electron.*, vol. 16, no. 3, pp. 390–399, 2001.
 [8] E. Tremblay, S. Atayde, and A. Chandra, "Comparative study of control strategies for the doubly fed induction generator in wind energy conversion systems: A DSP-based implementation approach," *IEEE Trans. Sustain. Energy*, vol. 2, no. 3, pp. 288–299, July 2011.
 [9] R. M. Prasad and M. A. Mulla, "Mathematical modeling and position-sensorless algorithm for stator-side field-oriented control of rotor-tied DFIG in rotor flux reference frame," *IEEE Trans. Energy Convers.*, vol. 35, no. 2, pp. 631–639, 2020.
 [10] M. W. K. Mbukani and N. Gule, "PLL-based sliding mode observer estimators for sensorless control of rotor-tied DFIG systems," *IEEE Trans. Ind. Appl.*, vol. 55, no. 6, pp. 5960–5970, Nov 2019.
 [11] B. Singh and N. K. S. Naidu, "Direct power control of single VSC-based DFIG without rotor position sensor," *IEEE Trans. Ind. Appl.*, vol. 50, no. 6, pp. 4152–4163, Nov 2014.